Since the relative variation of $d_\perp$ and $d_\parallel$ with the temperature is significant (Figure 2), the $r$ values calculated from the dipolar interaction are more accurate than those from $I_{rel}$ (eq II). Then, the difference between the $r$ values derived from spectra recorded at 293 and 77 K must be also significant. $r$ is equal to 0.51 nm at 293 K and changes to 0.55 nm when the spectra are recorded at 77 K. The $r$ values are independent of the Cu/Th atomic ratio (Cu/Th > 0.25).

It has been shown[3] that the copper (II) ion pairs are formed from one $Cu^{2+}$ ion occupying a substitutional bulk ($S_b$) site and another one present on the solid surface ($S_s$), which is easily reducible by hydrogen. Since the first species is very stable toward temperature and reactant agent, it seems that the variation of the distance $r$ in the copper(II) ion pairs versus the temperature is due only to the $Cu^{2+}$ ion which is accessible to the reduction. It is then evident to suppose that the copper(II) ion pairs in CuTh oxides are formed from two nonequivalent $Cu^{2+}$ ions.

It has been found[7] that if both ions were equivalent in the dimer and if the pair axis was the same as one of the principal axis of one single ion, the precursor of the dimeric species, the spectra corresponding to those monomer ions should have the same **g** tensor as the **g** tensor of the dimer and the splitting constant tensor of the dimeric spectrum should be half that of the single ion. In addition, the variation of the copper(II) ion pairs signal intensity versus the temperature can be studied. Indeed, the population $P$ of the triplet state will be governed by the Boltzmann distribution and the Curie law following the equation[8]

$$P = \frac{3}{T}\exp\left[\frac{-J}{kT}\right] \qquad (V)$$

By comparison of ESR spectra intensities recorded at 77 and 293 K of CuTh oxides, the $J$ value has been calculated from the above equation. This value ($J$ = 46.5 $cm^{-1}$) is larger than $A_{iso}$ (41.4 × $10^{-4}$ $cm^{-1}$) of the copper(II) ion pairs. Consequently,[9] the splitting constant of the single ion signal, if it is present, must be double that corresponding to copper(II) ion pairs. In fact, it is not the case for the ESR parameters of all signals previously characterized in CuTh oxides.[1,2] In particular, the $A_1$ signal has been attributed to $Cu^{2+}$ ions observed after reduction of the copper(II) ion pairs and found as its precursor. On the contrary, the two $Cu^{2+}$ ions of the pairs evidenced in $CeO_2$[10] were shown to be equivalent. A correlation between the precursor single ion and the copper(II) ion pairs has been established. The ESR parameters of the copper(II) ion pairs in $CeO_2$ did not change with the temperature as observed in the case of $ThO_2$.

In conclusion, it seems that if the two ions in one dimer are nonequivalent, the ESR parameters corresponding to this species change with temperature and no correlation can exist between the ESR spectra of the single ion and this dimer. In this case, eq I cannot describe correctly the system.

(6) Abragam, A.; Bleaney, B. *Electron Paramagnetic Resonance of Transition Ions*; Clarendon: Oxford, 1970; p 508.
(7) Mériaudeau, P.; Clerjaud, B.; Che, M. *J. Phys. Chem.* **1983**, *87*, 3872.
(8) Bleaney, B.; Bowers, K. D. *Proc. R. Soc. London, Ser. A.* **1952**, *214*, 451.
(9) Dupeyre, R. M.; Lemaire, A.; Rassat, A. *J. Am. Chem. Soc.* **1965**, *87*, 3771.
(10) Abou Kais, A.; Bennani, A.; Aissi, C. F.; Wrobel, G.; Guelton, M.; Vedrine, J. C., submitted to *J. Phys. Chem.*

# Metal Complexes in Inorganic Matrices. 7.[1] Nanometer-Sized, Uniform Metal Particles in a $SiO_2$ Matrix by Sol–Gel Processing of Metal Complexes

Boris Breitscheidel,[†] Jan Zieder,[‡] and Ulrich Schubert*[,†,‡]

*Institut für Anorganische Chemie der Universität Würzburg, Am Hubland, D-8700 Würzburg, Germany, and Fraunhofer-Institut für Silicatforschung, Neunerplatz 2, D-8700 Würzburg, Germany*

*Received February 5, 1991. Revised Manuscript Received March 25, 1991*

Composites containing nanometer-sized metal particles with a narrow particle size distribution, homogeneously dispersed in a $SiO_2$ matrix, are prepared by a three-step procedure: In the first step materials of the composition $L_nM[X(CH_2)_3SiO_{3/2}]_y \cdot xSiO_2$ (**4**) are obtained by sol–gel processing of an alkoxysilane of the type $X(CH_2)_3Si(OEt)_3$ (X = $NH_2$, $NHCH_2CH_2NH_2$, CN), a metal salt ($AgNO_3$, AgOAc, $Cd(NO_3)_2$, $Co(OAc)_2$, $Cu(OAc)_2$, $Ni(OAc)_2$, $Pd(acac)_2$, or $Pt(acac)_2$), and, optionally, $Si(OR)_4$. In the second step the polycondensates **4** are heated in air, and thereby the metal oxide/$SiO_2$ composites $MO_m \cdot (x + y)SiO_2$ (**5**, $MO_m$ = $Ag_2O$, CdO, CoO, CuO, NiO, PdO or PtO) are formed. The oxidation temperature is optimized by TGA. Reduction of the metal oxide particles of **5** by hydrogen in the third step produces nanocomposites $M \cdot (x + y)SiO_2$ (**6**, M = Ag, Co, Cu, Ni, Pd, or Pt). The metal particles in **6** are homogeneously distributed in the $SiO_2$ matrix. Depending on the metal and for some metals also on the metal loading, the metal particle sizes are in the range 2–60 nm, as determined by scanning transition electron microscopy. The smallest particles (2–4 nm) are obtained for Cu, Pd, and Pt. The particle size distribution is very narrow and of a Gaussian type. While the size of the metal particles and their size distribution in the Pd/$SiO_2$ composites is hardly affected by its metal content, the mean size of the metal particles in Ni/$SiO_2$ increases with increasing metal loading (from 5.9 nm for 2.7 wt % Ni to 57 nm for 44 wt % Ni). At low and high Ni content the particle size distribution is monomodal and, in between, a bimodal distribution is found.

## Introduction

The sol–gel route, originally directed toward the synthesis of purely inorganic materials from metal alkoxides, is increasingly extended to prepare organically modified materials by using organically substituted alkoxides, such as alkoxysilanes $RSi(OR')_3$. Materials with both interesting physical and chemical properties are obtained if the organic substituent R bears a functional or polymerizable group. The functional group may also be a metal complex

[†] University of Würzburg.
[‡] Fraunhofer-Institut.

0897-4756/91/2803-0559$02.50/0 

moiety ($L_nM$). Metal complexes of the type **1**, which contain at least one bifunctional ligand of the type X---$Si(OR)_3$, can be processed by the usual sol–gel procedure (eq 1). The bifunctional ligands consist of a group X

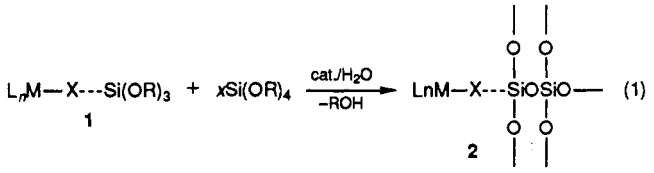

(1)

capable of coordinating $L_nM$ and a hydrolyzable silyl group, separated by an inert spacer (---). Co-condensation of **1** with $x$ equivalents of a network-forming reagent, such as $Si(OR)_4$ (TEOS), results in materials having the composition $L_nM$–X---$SiO_{3/2}$·$xSiO_2$ (**2**), in which the metal complex moiety is anchored to the silicate matrix via the spacer.

This approach of anchoring metal complex moieties to the silicate matrix was used to heterogenize catalytically active metal complexes.[2] In a preliminary communication we have reported that controlled degradation of certain palladium-containing compounds of the type **2** is an excellent method to get nanometer-sized and uniform palladium particles in $SiO_2$ (eq 2, R = $NH_2$ or $NHCH_2CH_2NH_2$, acac = acetylacetonate).[1a,3]

$$\mathrm{Pd(acac)_2 + 3RHN(CH_2)_3Si(OEt)_3 + xSi(OEt)_4} \xrightarrow{\mathrm{NH_3/H_2O}} \mathrm{[Pd(acac)_2{\cdot}3RHN(CH_2)_3SiO_{3/2}{\cdot}xSiO_2]} \xrightarrow[\mathrm{-H_2O/CO_2/NO}]{\mathrm{O_2/500\ ^\circ C}} \mathrm{PdO{\cdot}(3+x)SiO_2} \xrightarrow[\mathrm{-H_2O}]{\mathrm{H_2/30\ ^\circ C}} \mathrm{Pd{\cdot}(3+x)SiO_2} \quad (2)$$

Composites containing ultrafine metal particles of a controllable and uniform size in a ceramic matrix are very interesting materials not only as catalysts[4] but also for electronic applications, because they show quantum size effects,[5] particularly the size-induced metal–insulator transition (SIMIT).[6]

Small metal or metal oxide particles in ceramic matrices can be obtained from metal salts and hydrolyzable silicon or aluminum compounds by different methods.[4,7] However, one of the problems connected with these methods is the control of the metal particle size and the metal distribution. Ueno et al. found that hydrolysis of ethylene glycol solutions of TEOS and Ni, Fe, or Rh nitrate followed by calcination and reduction results in metal–$SiO_2$ composites with particularly small and homogeneous metal particles.[8] The key to control the metal particle size is a high dispersion of the metal compound during the polycondensation reaction, due to formation of M–O–Si links between the metal and the supporting matrix.

A more general approach to control dispersion of the metal compound during sol–gel processing is the use of chemically adjustable links between the metal ions and the $SiO_2$ support. Compounds of the type X---$Si(OR)_3$ meet these requirements. Since the anchoring group X and the spacer are necessary only to ensure a high, ideally molecular dispersion of the metal during polycondensation, their chemical composition must allow their complete removal during calcination. Therefore, the chemical link as well as the counteranion or ancillary ligands of the metal ion should ideally contain no elements other than carbon, nitrogen, oxygen, and hydrogen. In our investigations the silanes $X(CH_2)_3Si(OR)_3$ (R = Me, Et), X being a $NH_2$, $NHCH_2CH_2NH_2$, CN, or $CH(COMe)_2$ group, turned out to be suitable choices because these groups form a variety of stable complexes with most transition metals.

To prepare metal/$SiO_2$ composites using silanes X-$(CH_2)_3Si(OR)_3$ for coordinating the metal ions during polycondensation, three steps are necessary (eq 3): (i) sol–gel processing of metal complexes of type **3**, (ii) oxidation of the resulting polycondensates **4** to remove all organic parts and to get materials of the composition $MO_m$·$(x + y)SiO_2$ (**5**), and (iii) preparation of the composites M·$(x + y)SiO_2$ (**6**) by reduction of the metal oxide particles. In this paper we report details of the optimized procedures and the characterization of the compounds **3**–**6** for a representative number of transition metals.

$$\underset{\mathbf{3}}{\mathrm{L_nM[X(CH_2)_3Si(OR)_3]_y}} + x\mathrm{Si(OEt)_4} \xrightarrow[\mathrm{i}]{\mathrm{NH_3/H_2O}} \underset{\mathbf{4}}{\mathrm{L_nM[X(CH_2)_3SiO_{3/2}]_y{\cdot}xSiO_2}} \xrightarrow[\mathrm{ii}]{\mathrm{O_2T}} \underset{\mathbf{5}}{\mathrm{MO_m{\cdot}(x+y)SiO_2}} \xrightarrow[\mathrm{iii}]{\mathrm{H_2/T}} \underset{\mathbf{6}}{\mathrm{M{\cdot}(x+y)SiO_2}} \quad (3)$$

## Experimental Section

UV spectra were recorded on a Perkin-Elmer Lambda 15 UV–vis spectrophotometer. Thermogravimetric analyses were performed with a Du Pont thermal analyzer 9000, and BET measurements with a Micromeritics Sorptomat ASAP 2400. For STEM analyses a Phillips CN12-STEM was used.

**Polycondensation Reactions. General Procedure.** To a suspension of the corresponding metal salt in ethanol (2.5 mL of ethanol/0.1 mmol of salt for reactions without TEOS; 10 mL of ethanol/0.1 mmol of salt for reactions with TEOS) the specified amount of $X(CH_2)_3Si(OEt)_3$ (**7a**, X = $H_2NCH_2CH_2NH$; **7b**, X = $NH_2$; **7c**, X = CN) is added. The mixture is stirred at room temperature until a clear solution is obtained (about 1 h), the color of which depends on the kind of metal and ligand. After addition of the appropriate amount of TEOS, the calculated amount of aqueous 0.2 N ammonia, that corresponds to a 7.5-fold excess of water (relative to the amount of water necessary to hydrolyze all Si–OR groups; i.e., 7.5 $(4x + 3y)$ mmol of $H_2O$/mmol of metal) is added. The resulting homogeneous mixture, which shows the typical color of the corresponding metal complexes **3**, is heated to 70 °C for 72 h in a closed vessel. Then the solvent is removed at 60 °C and 12 Torr. (When the reaction mixture is not heated

(1) (a) Part 6: Schubert, U.; Breitscheidel, B.; Amberg-Schwab, S.; Buhler, H. *Ceramics Today—Tomorrow's Ceramics*; Vincenzini, P., Ed.; Elsevier Science: New York, in press. (b) Part 5: Egger, C.; Schubert, U. *Z. Naturforsch. Part B*, in press.

(2) Deschler, U.; Kleinschmit, P.; Panster, P. *Angew. Chem., Int. Ed. Engl.* **1986**, *25*, 236 and references therein. Schubert, U.; Egger, C.; Rose, K.; Alt, C. *J. Mol. Catal.* **1989**, *55*, 330.

(3) Schubert, U.; Amberg-Schwab, S.; Breitscheidel, B. *Chem. Mater.* **1989**, *1*, 576.

(4) Bond, G. C. *Surf. Sci.* **1985**, *156*, 966.

(5) Henglein, A. *Top. Curr. Chem.* **1988**, *143*, 113.

(6) Marquardt, P.; Börngen, L.; Nimtz, G.; Gleiter, H.; Sonnberger, R.; Zhu, J. *Phys. Lett.* **1986**, *114A*, 39. Marquardt, P.; Nimtz, G.; Mühlschlegel, B. *Solid State Commun.* **1988**, *65*, 539.

(7) Roy, R. A.; Roy, R. *Mater. Res. Bull.* **1984**, *19*, 169. Roy, R.; Komarneni, S.; Roy, D. M. *Mater. Res. Soc. Symp. Proc.* **1984**, *32*, 347. Subbanna, G. N.; Rao, C. N. R. *Mater. Res. Bull.* **1986**, *21*, 1465. Orgaz, F.; Rawson, H. *J. Non-Cryst. Solids* **1986**, *82*, 378.

(8) Ueno, A.; Suzuki, H.; Kotera, Y. *J. Chem. Soc., Faraday Trans. 1* **1983**, *79*, 127. Tohji, K.; Udagawa, Y.; Tanabe, S.; Ueno, A. *J. Am. Chem. Soc.* **1984**, *106*, 612. Tamagawa, H.; Oyama, K.; Yamaguchi, T.; Tanaka, H.; Tsuiki, H.; Ueno, A. *J. Chem. Soc., Faraday Trans. 1* **1987**, *83*, 3189. Tanabe, S.; Ida, T.; Suginage, T.; Ueno, A.; Kotera, Y.; Tohji, K.; Udagawa, Y. *Chem. Lett.* **1984**, 1567. Akiyama, T.; Tanigawa, E.; Ida, T.; Tsuiki, H.; Ueno, A. *Chem. Lett.* **1986**, 723. Seiji, T.; Koga, F.; Tanabe, S.; Ueno, A.; Kotera, Y. *Nippon Kagaku Kaishi* **1984**, 998; *Chem. Abstr.* **1984**, *101*, 44044a.

**Table I. Scale of the Polycondensation Reaction (Eq 3i)**

| | metal salt, g (mmol) | 7, g (mmol) | TEOS, g (mmol) | 0.2 N $NH_3$, mL (mmol) |
|---|---|---|---|---|
| **4a** | 3.40 (20.0) | 9.60 (40.0) | 8.91 (40.0) | 37.80 (2.1) |
| **4b** | 0.67 (4.0) | 1.84 (8.0) | 8.91 (40.0) | 24.80 (1.4) |
| **4c** | 1.23 (8.0) | 2.24 (8.0) | 8.91 (40.0) | 24.80 (1.4) |
| **4d** | 4.98 (20.0) | 5.60 (20.0) | | 8.10 (0.45) |
| **4e** | 3.99 (20.0) | 5.60 (20.0) | | 8.10 (0.45) |
| **4f** | 4.98 (20.0) | 5.60 (20.0) | | 8.10 (0.45) |
| **4g** | 4.98 (20.0) | 11.20 (40.0) | | 16.20 (0.9) |
| **4h** | 4.98 (20.0) | 16.80 (60.0) | | 24.30 (1.35) |
| **4i** | 1.25 (5.0) | 4.20 (15.0) | 2.78 (13.0) | 12.80 (0.7) |
| **4j** | 1.25 (5.0) | 4.20 (15.0) | 11.12 (50.0) | 33.08 (1.8) |
| **4k** | 0.50 (2.0) | 1.68 (6.0) | 13.40 (60.0) | 34.80 (1.9) |
| **4l** | 1.52 (5.0) | 2.80 (10.0) | | 4.05 (0.2) |
| **4m** | 0.91 (3.0) | 1.68 (6.0) | 1.67 (7.5) | 6.48 (0.4) |
| **4n** | 0.61 (2.0) | 1.12 (4.0) | 2.23 (10.0) | 7.02 (0.4) |
| **4o** | 0.46 (1.5) | 0.84 (3.0) | 3.34 (15.0) | 9.32 (0.5) |
| **4p** | 0.30 (1.0) | 0.56 (2.0) | 4.45 (20.0) | 11.61 (0.65) |
| **4q** | 0.16 (0.5) | 0.28 (1.0) | 3.34 (15.0) | 8.50 (0.5) |
| **4r** | 1.22 (4.0) | 5.60 (20.0) | 8.32 (40.0) | 29.70 (1.65) |
| **4s** | 0.98 (2.5) | 1.40 (5.0) | 16.70 (75.0) | 42.50 (2.4) |

**Table II. Elemental Analyses for the Polycondensates 4[a]**

| | C | H | N | metal |
|---|---|---|---|---|
| **4a** | 16.38 (17.46) | 2.45 (2.18) | 7.37 (7.63) | 20.65 (19.62) |
| **4b** | 10.37 (9.73) | 2.22 (1.93) | 3.67 (2.84) | 11.86 (10.93) |
| **4c** | 10.92 (10.50) | 3.08 (2.28) | 4.99 (4.90) | 7.57 (9.84) |
| **4d** | 32.83 (32.72) | 5.53 (5.76) | 8.53 (8.48) | 16.06 (17.84) |
| **4e** | 31.99 (32.27) | 5.78 (5.68) | 8.05 (8.37) | 17.60 (18.99) |
| **4f** | 31.04 (32.74) | 6.38 (5.76) | 7.76 (8.49) | 15.80 (17.79) |
| **4g** | 35.41 (34.79) | 7.52 (6.63) | 11.25 (11.60) | 10.66 (12.16) |
| **4h** | 34.35 (35.85) | 7.85 (7.08) | 12.72 (13.21) | 8.50 (9.23) |
| **4i** | 26.97 (29.01) | 6.37 (5.73) | 10.39 (10.69) | 7.22 (7.47) |
| **4j** | 18.73 (18.45) | 3.86 (3.64) | 6.79 (6.80) | 4.29 (4.75) |
| **4k** | 10.04 (9.36) | 2.41 (1.85) | 3.52 (3.45) | 2.13 (2.40) |
| **4l** | 32.32 (39.32) | 6.73 (6.55) | 9.58 (9.17) | 19.61 (17.43) |
| **4m** | 28.06 (31.56) | 5.55 (5.26) | 8.10 (7.36) | 14.31 (13.99) |
| **4n** | 26.32 (26.36) | 4.51 (4.39) | 6.35 (6.15) | 11.76 (11.69) |
| **4o** | 18.30 (19.83) | 3.69 (3.30) | 5.58 (4.63) | 8.33 (8.79) |
| **4p** | 12.56 (13.26) | 2.79 (2.21) | 3.83 (3.09) | 5.35 (5.88) |
| **4q** | 10.78 (9.96) | 2.41 (1.66) | 2.75 (2.32) | 4.48 (4.41) |
| **4r** | 18.76 (20.85) | 4.96 (4.73) | 8.20 (8.39) | 5.72 (6.37) |
| **4s** | 10.61 (9.60) | 2.28 (1.60) | 1.96 (2.24) | 6.37 (7.81) |

[a] The calculated values (in parentheses) correspond to the ideal composition according to the formulas.

**Table III. Reaction Conditions for the Oxidation Step (Preparation of 5) and Reduction Step (Preparation of 6)**

| | oxidn of 4 (prep of 5) | | redn of 5 (prep of 6) |
|---|---|---|---|
| **5a** | 400 °C/20 min[a] | **6a** | 500 °C/2 h |
| **5b** | 500 °C/30 min[a] | **6b** | 500 °C/2 h |
| **5c** | 550 °C/50 min[a] | | |
| **5d** | 500 °C/30 min[a] | **6d** | 500 °C/2 h |
| **5e** | 400 °C/30 min[a] | **6e** | 500 °C/2 h |
| **5f** | 500 °C/30 min[a] | **6f** | 500 °C/2 h |
| | | **6f'** | 900 °C/4 h |
| **5g** | 500 °C/30 min | **6g** | 900 °C/2 h |
| **5h** | 500 °C/30 min | **6h** | 900 °C/2 h |
| **5i** | 550 °C/30 min | **6i** | 900 °C/2 h |
| **5j** | 550 °C/30 min | **6j** | 900 °C/2 h |
| **5k** | 550 °C/30 min | **6k** | 900 °C/2 h |
| **5l** | 400 °C/20 min[a] | **6l** | 25 °C/1 h |
| **5m** | 550 °C/30 min | **6m** | 25 °C/1 h |
| **5n** | 550 °C/30 min | **6n** | 25 °C/1 h |
| **5o** | 550 °C/30 min | **6o** | 25 °C/1 h |
| **5p** | 550 °C/30 min | **6p** | 25 °C/1 h |
| **5q** | 550 °C/30 min[a] | **6q** | 25 °C/1 h |
| **5r** | 550 °C/30 min | **6r** | 500 °C/1 h |
| **5s** | 500 °C/30 min | **6s** | 500 °C/1 h |

[a] Optimized by TGA.

before evaporation of the solvent, part of silicon is lost due to volatile silicon compounds.) The obtained solid, chemically homogeneous xerogels **4a–s** (Chart I), are dried at 70 °C and $10^{-3}$ Torr to remove adsorbed water and alcohol. The scale of the reactions is specified in Table I. Elemental analyses of the polycondensates **4** are given in Table II.

**Oxidation of 4.** The polycondensates **4** are placed in a horizontal quartz tube and heated in an tube oven Heraeus ROK/A 4/60 at the conditions specified in Table III. A stream of 200 mL/min of dry air is maintained during heating. Elemental analyses of the obtained composites **5** are given in Table IV.

**Reduction of 5.** The composites **5** are placed in a horizontal quartz tube and heated under hydrogen in an tube oven Heraeus ROK/A 4/60 at the conditions specified in Table III. A stream of 200 mL/min of hydrogen is maintained during heating. Elemental analyses of the obtained composites **6** are given in Table V.

Metal oxide and metal particle sizes in the composites **5** and **6** were determined by STEM and are given in Table VI. Table VII contains the specific surface areas of the compounds **4–6** as determined by the BET method, and Table VIII (supplementary material; see the paragraph at the end of the paper) pore radii and pore volumes.

## Results and Discussion

**Step 1: Polycondensation.** In light of a simple, general, and practical material synthesis, the use of isolated metal complexes of the type **3** is not very reasonable. We therefore decided to prepare the metal complexes in situ from metal salts and $X(CH_2)_3Si(OEt)_3$ (**7a**, X = $H_2NCH_2CH_2NH$; **7b**, X = $NH_2$; **7c**, X = CN). In a typical experiment, the metal salt and $y$ equivalents of **7** are dissolved in ethanol. After the corresponding complex is formed, $x$ equivalents of TEOS (optionally) and the calculated amount of 0.2 N aqueous ammonia are added. Aqueous ammonia provides both the water necessary for hydrolysis and ammonia as the polycondensation catalyst. Solid, chemically homogeneous polycondensates **4a–s** are obtained after workup. By the metal/TEOS ratio in the starting mixture, the metal loading in the final materials is controlled. The largest possible metal loading is reached only if the metal salt and the minimum amount of **7** necessary for coordination of the metal ion are used.

Elemental analyses (Table II) correspond reasonably well to the ideal compositions but need to be commented on: The hydrogen values are consistently higher than those calculated, because the compounds still contain some adsorbed water or SiOH groups in this stage. The fact that for most polycondensates the metal content is lower than in the idealized formulas is due to a higher oxygen content (since no other elements than C, H, N, O, and metal are present from the beginning, the diffence between the sum of the found C, H, N, and metal values and 100% corresponds to the oxygen content). A higher oxygen content could be caused by the adsorbed water or by partial oxidation of the metal. Correct carbon values are nevertheless found because the higher oxygen content is compensated by some remaining Si–OR groups due to incomplete hydrolysis.

In the present study the ethylenediamine derivative $H_2NCH_2CH_2NH(CH_2)_3Si(OEt)_3$ (**7a**) proved to be very effective for anchoring the metal ions of $Cd(NO_3)_2$, $Co(OAc)_2$, $Cu(OAc)_2$, $Ni(OAc)_2$ (OAc = acetate), $Pd(acac)_2$, and $Pt(acac)_2$ to the matrix, whereas $AgNO_3$ was better coordinated by $H_2N(CH_2)_3Si(OEt)_3$ (**7b**) or $NC(CH_2)_3Si(OEt)_3$ (**7c**). The use of the acetylacetonate derivative $(Me(O)C)_2CH(CH_2)_3Si(OR)_3$ is under investigation.[9] For $Co(OAc)_2$, $Cu(OAc)_2$, and $Ni(OAc)_2$ 1 equiv of **7a** is enough to

(9) Urbaniak, W.; Schubert, U. Submitted to *Organometallics*.

**Chart I**[a]

| | $LnM[X(CH_2)_3SiO_{3/2}]_y \cdot xSiO_2$ 4 | $MO_m \cdot (x + y)SiO_2$ 5 | $M \cdot (x + y)SiO_2$ 6 |
|---|---|---|---|
| a | $Ag(NO_3) \cdot 2NC\text{-}Y \cdot 2SiO_2$ | $Ag_2O \cdot 8SiO_2$ | $Ag \cdot 4SiO_2$ |
| b | $Ag(OAc) \cdot 2H_2N\text{-}Y \cdot 10SiO_2$ | $Ag_2O \cdot 24SiO_2$ | $Ag \cdot 12SiO_2$ |
| c | $Cd(NO_3)_2 \cdot 2H_2NCH_2CH_2NH\text{-}Y \cdot 10SiO_2$ | $CdO \cdot 12SiO_2$ | |
| d | $Co(OAc)_2 \cdot H_2NCH_2CH_2NH\text{-}Y$ | $CoO \cdot SiO_2$ | $Co \cdot SiO_2$ |
| e | $Cu(OAc)_2 \cdot H_2NCH_2CH_2NH\text{-}Y$ | $CuO \cdot SiO_2$ | $Cu \cdot SiO_2$ |
| f | $Ni(OAc)_2 \cdot H_2NCH_2CH_2NH\text{-}Y$ | $NiO \cdot SiO_2$ | $Ni \cdot SiO_2$ |
| g | $Ni(OAc)_2 \cdot 2H_2NCH_2CH_2NH\text{-}Y$ | $NiO \cdot 2SiO_2$ | $Ni \cdot 2SiO_2$ |
| h | $Ni(OAc)_2 \cdot 3H_2NCH_2CH_2NH\text{-}Y$ | $NiO \cdot 3SiO_2$ | $Ni \cdot 3SiO_2$ |
| i | $Ni(OAc)_2 \cdot 3H_2NCH_2CH_2NH\text{-}Y \cdot 2.5SiO_2$ | $NiO \cdot 5.5SiO_2$ | $Ni \cdot 5.5SiO_2$ |
| j | $Ni(OAc)_2 \cdot 3H_2NCH_2CH_2NH\text{-}Y \cdot 10SiO_2$ | $NiO \cdot 13SiO_2$ | $Ni \cdot 10SiO_2$ |
| k | $Ni(OAc)_2 \cdot 3H_2NCH_2CH_2NH\text{-}Y \cdot 30SiO_2$ | $NiO \cdot 33SiO_2$ | $Ni \cdot 33SiO_2$ |
| l | $Pd(acac)_2 \cdot 2H_2NCH_2CH_2NH\text{-}Y$ | $PdO \cdot 2SiO_2$ | $Pd \cdot 2SiO_2$ |
| m | $Pd(acac)_2 \cdot 2H_2NCH_2CH_2NH\text{-}Y \cdot 2.5SiO_2$ | $PdO \cdot 4.5SiO_2$ | $Pd \cdot 4.5SiO_2$ |
| n | $Pd(acac)_2 \cdot 2H_2NCH_2CH_2NH\text{-}Y \cdot 5SiO_2$ | $PdO \cdot 7SiO_2$ | $Pd \cdot 7SiO_2$ |
| o | $Pd(acac)_2 \cdot 2H_2NCH_2CH_2NH\text{-}Y \cdot 10SiO_2$ | $PdO \cdot 12SiO_2$ | $Pd \cdot 12SiO_2$ |
| p | $Pd(acac)_2 \cdot 2H_2NCH_2CH_2NH\text{-}Y \cdot 20SiO_2$ | $PdO \cdot 22SiO_2$ | $Pd \cdot 22SiO_2$ |
| q | $Pd(acac)_2 \cdot 2H_2NCH_2CH_2NH\text{-}Y \cdot 30SiO_2$ | $PdO \cdot 32SiO_2$ | $Pd \cdot 32SiO_2$ |
| r | $Pd(acac)_2 \cdot 5H_2NCH_2CH_2NH\text{-}Y \cdot 10SiO_2$ | $PdO \cdot 15SiO_2$ | $Pd \cdot 15SiO_2$ |
| s | $Pt(acac)_2 \cdot 2H_2NCH_2CH_2NH\text{-}Y \cdot 30SiO_2$ | $PtO \cdot 32SiO_2$ | $Pt \cdot 32SiO_2$ |

[a] $Y = (CH_2)_3SiO_{3/2}$.

**Table IV. Elemental Analyses for the Metal Oxide/$SiO_2$ Composites 5[a]**

| | found | | | |
|---|---|---|---|---|
| | C | H | N | metal found (calcd) |
| **5a** | 0.54 | 0.25 | 0.00 | 28.50 (30.32) |
| **5b** | 1.29 | 0.42 | 0.12 | 14.95 (12.91) |
| **5c** | 1.19 | 0.58 | 0.63 | 9.53 (13.28) |
| **5d** | 0.00 | 0.00 | 0.00 | 42.33 (43.66) |
| **5e** | 0.00 | 0.19 | 0.00 | 40.45 (45.52) |
| **5f** | 0.23 | 0.46 | 0.00 | 36.84 (43.57) |
| **5g** | 0.31 | 0.95 | 0.00 | 24.82 (30.15) |
| **5h** | 0.49 | 0.44 | 0.09 | 17.77 (23.05) |
| **5i** | 0.23 | 0.54 | 0.27 | 13.29 (14.48) |
| **5j** | 0.29 | 0.32 | 0.26 | 6.54 (6.87) |
| **5k** | 0.59 | 0.59 | 0.23 | 2.71 (2.86) |
| **5l** | 0.18 | 0.12 | 0.00 | 40.49 (43.89) |
| **5m** | 0.77 | 0.29 | 0.32 | 25.37 (27.09) |
| **5n** | 1.08 | 0.36 | 0.34 | 17.70 (19.60) |
| **5o** | 0.45 | 0.31 | 0.38 | 11.68 (12.62) |
| **5p** | 0.23 | 0.52 | 0.27 | 6.84 (7.37) |
| **5q** | 0.57 | 0.52 | 0.40 | 4.93 (5.21) |
| **5r** | 0.15 | 0.57 | 0.00 | 8.57 (10.41) |
| **5s** | 0.34 | 0.96 | 0.00 | 8.37 (9.16) |

[a] The calculated metal content corresponds to the ideal composition according to the formulae. The theoretical values for C, H, and N are zero.

**Table V. Elemental Analyses for the Metal/$SiO_2$ Composites 6[a]**

| | found | | | |
|---|---|---|---|---|
| | C | H | N | metal found (calcd) |
| **6a** | 0.14 | 0.18 | 0.00 | 28.70 (31.01) |
| **6b** | 1.18 | 0.32 | 0.10 | 10.22 (13.03) |
| **6d** | 0.07 | 0.00 | 0.00 | 47.51 (49.54) |
| **6e** | 0.11 | 0.00 | 0.00 | 46.17 (51.42) |
| **6f** | 0.22 | 0.48 | 0.00 | 43.70 (49.44) |
| **6f′** | 0.26 | 0.30 | 0.00 | 43.95 (49.44) |
| **6g** | 0.28 | 0.04 | 0.19 | 31.08 (32.85) |
| **6h** | 0.72 | 0.00 | 0.00 | 20.05 (24.59) |
| **6i** | 0.29 | 0.00 | 0.19 | 14.01 (15.08) |
| **6j** | 0.25 | 0.06 | 0.15 | 6.99 (7.00) |
| **6k** | 0.77 | 0.00 | 0.20 | 2.65 (2.88) |
| **6l** | 0.10 | 0.26 | 0.00 | 44.81 (47.00) |
| **6m** | 0.30 | 0.34 | 0.30 | 26.03 (28.24) |
| **6n** | 0.51 | 0.45 | 0.35 | 18.12 (20.20) |
| **6o** | 0.22 | 0.35 | 0.33 | 10.84 (12.87) |
| **6p** | 0.29 | 0.56 | 0.26 | 7.18 (7.46) |
| **6q** | 0.53 | 0.60 | 0.33 | 5.52 (5.25) |
| **6r** | 0.08 | 0.22 | 0.00 | 9.36 (10.57) |
| **6s** | 0.22 | 0.40 | 0.00 | 7.93 (9.23) |

[a] The calculated metal content corresponds to the ideal composition according to the formulae. The theoretical values for C, H, and N are zero.

effectively fix the metal to the support, whereas 2 equiv is necessary for $Pd(acac)_2$ and $Pt(acac)_2$. With smaller amounts of **7** (=$y$), metal ions are eluted upon washing **4** with water and alcohol. Complexes formed from $Pd(acac)_2$ or $Ag^+$ with only 1 equiv of **7** are not stable during polycondensation, and colloidal metal with uncontrollable metal particle sizes is formed.

When TEOS is hydrolyzed in the presence of the metal salts without using the anchoring ligands **7**, the metal ions are eluted when the resulting xerogels are washed with water or alcohols. From this fact and due to the typical colors of the compounds **4**, it is obvious that metal complexes, which are anchored to the silicate matrix via the propylene chain, are formed. Except for the nickel compounds **4f–k** we did not determine the exact formulation of the metal complexes. Since **4f–k** are insoluble, we compared the solid-state UV spectra with those of soluble complexes obtained from $Ni(OAc)_2$ and ethylenediamine ($H_2NCH_2CH_2NH_2$, "en").

The UV spectra of $[Ni(H_2O)_4(en)]^{2+}$, $[Ni(H_2O)_2(en)_2]^{2+}$, and $[Ni(en)_3]^{2+}$ are distinctly different from each other: the absorption maxima are shifted to higher wavelengths as the number of en ligands decreases.[10] When 1 or 2 equiv of **7a** is added to an ethanolic solution of $Ni(OAc)_2$ (Figure 1a), the UV spectra ($y$ = 1, $\nu_{max}$ 637, 382 nm; $y$ = 2, $\nu_{max}$ 582, 361 nm) are nearly identical with those of the corresponding en complexes in ethanol. Adding a third equivalent **7a** to the solution does not change the spectrum (Figure 1a), i.e., even with an excess of **7a** only complexes of the composition $[Ni(EtOH)_2(\mathbf{7a})_2]^{2+}$ are formed. This is in contrast to the corresponding en complexes, where $[Ni(en)_3]^{2+}$ is formed under the same conditions.

The only difference between the UV spectra of solutions containing $Ni(OAc)_2$ and $y$ equivalents of **7a** ($y$ = 1–3) and the corresponding solid polycondensates is a minor shift of the bands to higher wavelengths upon polycondensation (Figure 1b). We are unable to decide whether in the polycondensates alcohol is still coordinated to the metal or has been replaced by SiOH groups or unhydrolyzed SiOEt

(10) *Gmelins Handbuch der Anorganischen Chemie*; Verlag Chemie: Weinheim 1968; Part 57, C1, p 149.

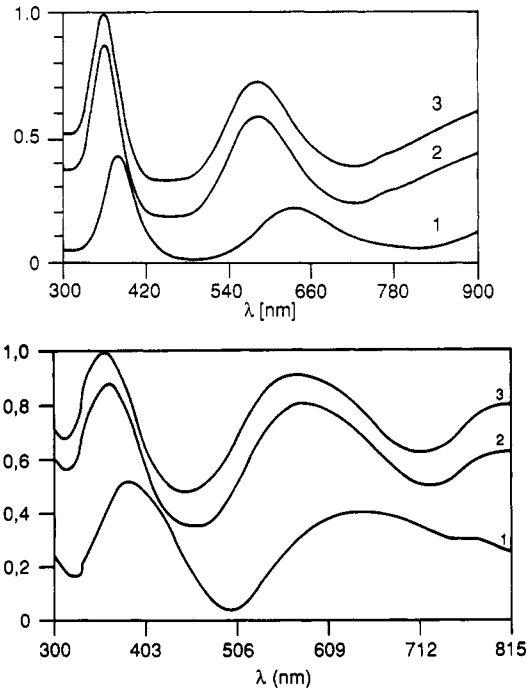


**Figure 1.** (a, top) UV spectra of $Ni(OAc)_2$ and $y$ equivalents of **7a** in ethanol solution. Curve 1, $y = 1$; curve 2, $y = 2$; curve 3, $y = 3$. (b, bottom) UV spectra of the solid polycondensates obtained from solutions containing $Ni(OAc)_2$ and $y$ equivalents of **7a**. Curve 1, $y = 1$; curve 2, $y = 2$; curve 3, $y = 3$.

groups of the matrix. However, the general type of complex is the same in the solid state and in solution. While the spectra for $y = 2$ and $y = 3$ are identical in solution, they are slightly different for the corresponding polycondensates ($y = 3$, $\nu_{max}$ 574, 360 nm; $y = 2$, $\nu_{max}$ 583, 364 nm; $y = 1$, $\nu_{max}$ 646, 388 nm). Although the wavelength shift is smaller than for complexes of the type $[Ni(en)_n(H_2O)_{6-2n}]^{2+}$, it appears possible that during polycondensation complexes of the type $\{Ni[H_2NCH_2CH_2CH_2NH(CH_2)_3SiO_{3/2}]_3\}^{2+}$ are additionally formed.

The UV spectra clearly show that the conception of in situ formation of metal complexes during polycondensation of metal salts and silanes of the type **7** is valid. Although the complexes $L_nM[X(CH_2)_3Si(OR)_3]_y$ (**3**) are also formed by stoichiometric reaction of the metal salts with the silanes **7**, they proved to be very moisture sensitive and therefore were difficult to isolate analytically pure. For the preparation of the composites **5** and **6** the "in situ method" described here is more practical than using preformed metal complexes.

**Step 2: Oxidation.** In the second step of the synthesis the metal oxide/$SiO_2$ composites **5** are prepared by heating the corresponding polycondensates **4** in air (eq 3ii). The organic parts, having served the purpose of anchoring the metal complexes to the silicate matrix and providing a high metal dispersion, are oxidatively removed.

The oxidation temperature should be high enough to ensure the complete removal of all organic parts but not higher than necessary to avoid an excessive sintering of the metal compound. Mass spectroscopic analysis of the oxidation products ($CO_2$, NO, and $H_2O$) of a sample of **4**, prepared from $Pd(acac)_2$, **7b**, and TEOS (molar ratio 1:3:8), shows that up to about 170 °C only water is removed (Figure 2). Oxidation and/or thermolysis of the organic parts then occurs in several steps and is complete at 500 °C. At higher temperatures only water is detected. Obviously, some of the water produced during oxidation of the organic moieties is adsorbed by the very hygroscopic silica matrix and is liberated only at higher temperatures.

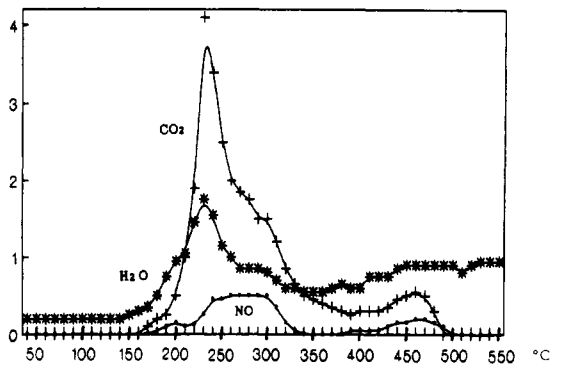


**Figure 2.** Temperature-programmed mass spectroscopic analysis of the oxidation products of **4**, prepared from $Pd(acac)_2$, **7b**, and TEOS (molar ratio 1:3:8).

The best temperature for oxidation is routinely determined by thermogravimetric analyses. The polycondensates **4** are slowly heated in air until a weight constancy is reached. Since exposure to high temperatures should be as short as possible to limit particle growth, the exposure time is also optimized by rapidly heating **4** to the predetermined best temperature and recording the time in which a weight constancy is reached. In Table III the optimized conditions for the oxidation step are given.

Oxidation of the polycondensates **4** was performed by placing them in a horizontal quartz tube and heating them in a furnace, while dry air was passed over the sample. Elemental analysis of the composites **5** (Table IV) show that with very few exceptions the carbon content is distinctly below 1% and the nitrogen content below 0.5%. The residual carbon and nitrogen content is due to the way in which the oxidation was carried out. If a better contact between the sample and air is provided, the carbon and nitrogen content drops to zero under the same conditions. The hydrogen content of **5** is rather high due to the adsorbed water. As discussed for **4**, the metal content is lower than calculated for the idealized composition, owing to the adsorbed water and the residual organic parts.

Inspection of Table III shows that the lowest possible, best temperatures for complete oxidation depend on the metal and on the nature and the amount of the organic moieties used to bind the metal ions. As a comparison, for complete oxidative removal of all organic parts from $H_2NCH_2CH_2NH(CH_2)_3SiO_{3/2}$, prepared by polycondensation of **7a** in the absence of a metal, 650 °C for 35 min is necessary. The metals seemingly act as oxidation catalysts, because complete oxidation occurs at lower temperatures. Cu and Ag are particularly effective in this respect. Interestingly, a clear dependency on the metal complex/$SiO_2$ ratio is found (for example **4l** vs **4q**). With a high metal complex concentration, i.e., a high concentration of **7** in the starting mixture, lower temperatures are sufficient. We attribute this behavior to the different porosities (vide infra) or to the promotion of the oxidation by higher metal concentrations.

The metal oxide particle sizes in **5** will be commented on in the next paragraph.

**Step 3: Reduction.** In the final step, the metal/$SiO_2$ composites **6** are prepared by the reduction of the metal oxide particles of **5** by hydrogen (eq 3iii). During reduction the color of the composites changes from that of the metal oxides to gray or black. The same conditions were chosen as for the reduction of the corresponding bulk oxides, because the reaction conditions for this step are difficult to optimize and the completeness of reduction is not easy to monitor by routine methods. The necessary temperatures depend on the metal (Table III). The CdO/$SiO_2$

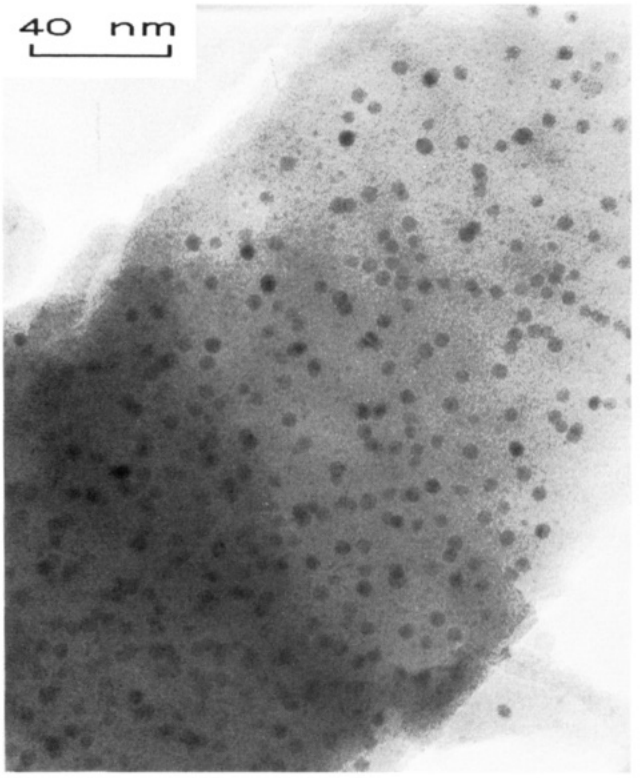


**Figure 3.** Scanning transition electron micrograph of composite **6r**. Mean particle diameter: 3.8 nm.

composite **5c** cannot be reduced without substantial loss of Cd, because Cd is rather volatile at the necessary reduction temperatures. Elemental analyses of the composites **6** are given in Table V.

We have no direct evidence for the *completeness* of the reduction step. Indirect evidence stems from the fact that the Pd- and Ni-containing composites are catalysts for the hydrogenation of olefins (some of the Pd composites are even more active than commercially available Pd-on-charcoal).[11] The composites **6** with a high metal loading (**6a**, **6d**, **6e**, **6f**, and **6l**) show the SIMIT effect (measured by microwave absorption).[12] A detailed discussion of the applications for the composites **6** is beyond the scope of this article and will be published elsewhere. Although both catalytic and SIMIT activity prove that the particles are, in principle, metallic, they do not prove that they are *entirely* metallic in any case. Assuming a complete reduction appears reasonable for the nobler metals. However, we cannot exclude that there is a metal–support interaction, i.e., an oxide layer at the metal/$SiO_2$ interface, for the particles of the less noble metals. In the Ni/$SiO_2$ composite **6f** a weak band is observed in the IR spectrum at 960 $cm^{-1}$, which was assigned to a Ni–O–Si vibration.[8] This band disappears when the reduction is carried out at 900 °C (composite **6f′**) instead of 500 °C, indicating that only at this temperature are residual Ni–O–Si links reduced. A powder diffraction pattern analysis of **6f′** showed metallic nickel as the only crystalline phase. However, this method also is not suited to give a definite answer on whether reduction is complete or not, because NiO domains might be amorphous or too small to detect.

Metal–support interaction is difficult to determine without prior knowledge of the noninteracting particles. Although the importance of such interactions and their relevance to particular applications of **6** still has to be clarified, the present results clearly show the presence of metallic particles in the composites **6**.

(11) Breitscheidel, B.; Schubert, U., unpublished.
(12) Marquardt, P.; Nimtz, G.; Breitscheidel, B.; Schubert, U., unpublished.

**Table VI. Metal Oxide and Metal Particle Sizes**

| | min and max particle diams, nm | mean particle diam, nm |
|---|---|---|
| **5f** | 22.5–47.4 | 34.8 |
| **5k** | 0.3–2.7 | 1.4 |
| **6a** | 9.0–30.9 | 19.5 |
| **6d** | 11.0–24.9 | 17.4 |
| **6e** | 1.5–7.4 | 3.9 |
| **6f** | 37.5–62.4 | 50.3 |
| **6f′** | 32.5–102.4 | 57 |
| **6g**[a] | 7.5–12.4, 27.5–72.4 | |
| **6h**[a] | 2.5–22.4, 62.5–102.4 | |
| **6i**[a] | 2.5–12.4, 32.5–57.4 | |
| **6j** | 12.5–47.4 | 22.9 |
| **6k** | 2.5–12.4 | 5.9 |
| **6l** | 1.8–4.2 | 3.0 |
| **6n** | 1.8–4.2 | 2.8 |
| **6q** | 1.3–3.7 | 2.4 |
| **6r** | 2.8–5.2 | 3.8 |
| **6s** | 0.8–4.2 | 2.5 |

[a] Bimodal particle distribution.

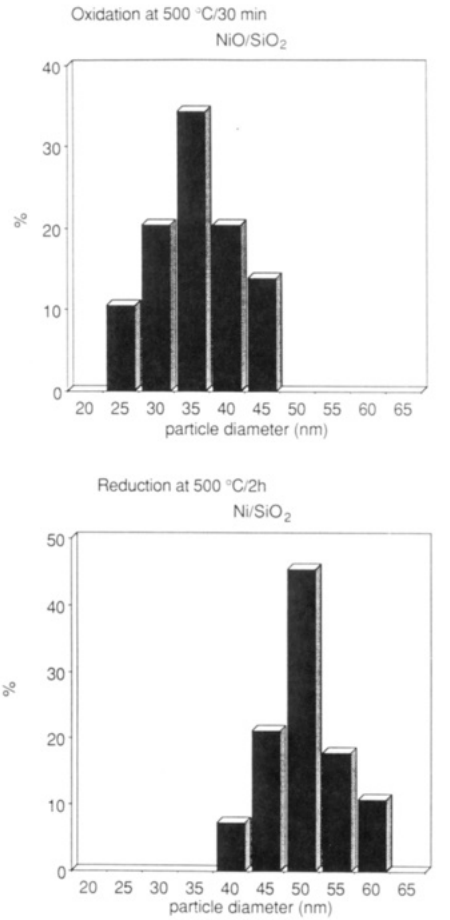


**Figure 4.** Metal-particle diameter distribution of the composite NiO·$SiO_2$ (**5f**) and the composite Ni·$SiO_2$ (**6f**).

The metal particle sizes were analyzed by scanning transition electron micrograph (STEM). A typical STEM photograph (composite **6r**) is shown in Figure 3. It shows the high and homogeneous disperison of the metal *throughout* the $SiO_2$ matrix. The particles are well separated from each other, and their diameters are very small and uniform, even in the materials with high metal loadings. By measuring the diameters of about 50–100 particles in each STEM photograph, the particle size distributions were determined. They all are very narrow and approx-

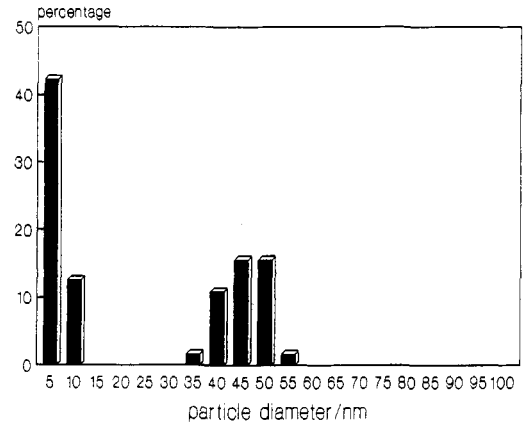


**Figure 5.** Metal-particle diameter distribution of the composite **6i** (14 wt % Ni).

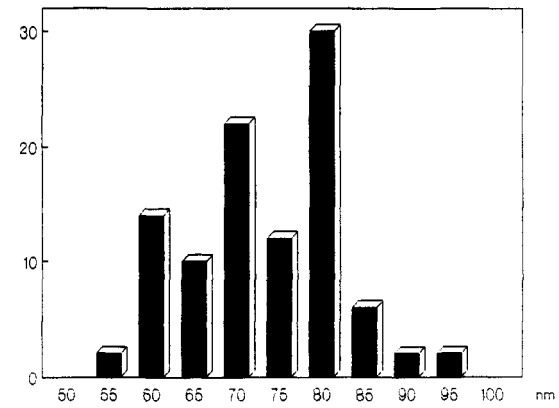


**Figure 6.** Ni particle size distribution of the composite Ni-$SiO_2$ (52 wt % Ni) prepared from $Ni(OAc)_2$, $H_2N(CH_2)_2NH_2$, and TEOS (ratio 1:1:1). The average particle diameter is 75 nm.

imately normal distributed. The minimum, maximum, and mean particle sizes of representative examples of **6** are listed in Table VI; a typical diagram (that of **6f**) is shown in Figure 4. The other diagrams are deposited as supplementary material.

As expected, the particle sizes depend very strongly on the kind of metal. Very small metal particles (2–4 nm) are obtained for Cu (**6e**), Pd (**6l–r**), and Pt (**6s**). According to model calculations,[4] Pd particles of 2-nm (4-nm) diameter correspond to 285 (2279) atoms if the particles are spheres, or 544 (4354) atoms if they are cubes, corresponding to a dispersion of 61.1 (30.4) or 51.2% (25.6%), respectively. Similar values were calculated for Pt. The similarity in size with giant palladium clusters of the idealized composition $Pd_{561}(phen)_{60}(OAc)_{180}$ (phen = 1,10-phenanthroline)[13] is also noteworthy. In these clusters the icosahedral (charged!) metal skeleton is 2.5 nm in diameter.

The metal loading of **5** and **6** is governed by the ratio of the starting compounds; its upper limit is reached if polycondensation of **7** and the metal salt is carried out without TEOS. For Ag, Co, and Cu, we prepared only composites with the largest possible metal loading; for Pd and Ni, we also determined the dependency between metal loading and mean particle size. The mean Pd particle diameter in **6** is rather independent of the metal loading (Table VI, **6l,n,q**): it increases only slightly from about 2.4 nm (**6q**, 5.5 wt % Pd) to 3.0 nm (**6l**, 45% Pd). In **6l**, with high metal loading, the metal particles are still well separated from each other and the particle size distribution curve is narrow (1.8–4.2 nm) and approximately Gaussian-shaped. The particle size is affected to only a minor extent by the reduction temperature: if **5l** is reduced at 500 °C for 2 h (instead of 25 °C), the mean particle size in **6l** increases only to 3.5 nm (particles from 1.5 to 5.4 nm).

Contrary to the Pd/$SiO_2$ composites, there is a clear relation between the particle sizes and both the metal loading and the reduction temperature in the Ni/$SiO_2$ composites (**6f–k**). At a low metal loading (**6k,j**: 2.7 and 7.0% Ni) there is a monomodal particle size distribution; the mean particle diameter increases with increasing metal loading (from 5.9 nm in **6k** to 22.9 nm in **6j**). Further increasing the metal loading results in a bimodal particle size distribution, the smaller particles centered around 5–10 nm and the larger ones around 40–90 nm (e.g., **6i**, Figure 5). The percentage of larger particles increases with increasing metal loading, until a monomodal distribution is reached again at the maximum metal loading (**6f'**, 44% Ni), but with larger particles (mean size 57 nm). A higher reduction temperature causes partial sintering of the metal: compared with **6f**, the average particle size in **6f'** is only slightly larger (57 instead of 50 nm), but the particle size distribution curve is spread (33–102 nm) and no longer normal distributed.

Since temperatures for the reduction of the Pd-containing composites are very low, we assume that the PdO particle size distribution in the PdO/$SiO_2$ composites **5l–r** is about the same as in the Pd/$SiO_2$ composites **6l–r**. To find out whether reduction at higher temperatures causes changes in the particle size distribution, we also determined the particle sizes of two representative NiO/$SiO_2$ composites (**5f** and **5k**, Table VI, Figure 4). In both cases the particle sizes slightly increase during reduction (**5f**, 34.8 nm; **6f**, 50.3 nm [reduction at 500 °C]; **5k**, 1.4; **6k**, 5.9 nm [reduction at 900 °C]), but the shape and width of the particle size distribution curve remain about the same. A comparison between **5k/6k** and **5f/6f'** also shows that the effect of the higher temperature on the particle size distribution is less pronounced when the metal loading is low.

The final question is whether the complexation of the metal and anchoring of the metal complex via the ligands **7** to the $SiO_2$ matrix during polycondensation is indeed essential for obtaining composites **5** and **6** with small particles and narrow particle distributions. We therefore prepared a Ni/$SiO_2$ composite with the same composition as **6f**, but instead of using $Ni(OAc)_2$ and 1 equiv of **7a**, we reacted $Ni(OAc)_2$, 1 equiv of ethylenediamine (en), and 1 equiv of TEOS. The reaction conditions during polycondensation, oxidation, and reduction were the same, so as to avoid any influence of these parameters on the results. The Ni particle size distribution of the composite obtained without using **7a** is shown in Figure 6. The advantage of using silanes of the type $X(CH_2)_nSi(OR)_3$ (**7**) to prepare small and uniform metal particles in $SiO_2$ is obvious, and the difference between Figures 4 and 6 does not need any comment. Although narrow particle size distributions have occasionally been reported for a few metal/$SiO_2$ nanocomposites prepared from metal salts and TEOS alone,[7] these results cannot be generalized. More typically, distribution curves similar to those shown in Figure 6 are obtained on the basis of our experience. Our method for preparing metal/$SiO_2$ nanocomposites using silanes of the type **7** gives narrow particle size distributions in every case investigated so far.

**Porosity of the Materials.** Apart from complexing the metal ions, the silanes **7** used for the synthesis of the polycondensates **4** also have an important influence on the porosity of the composites **5** and **6**.

(13) Vargaftik, M. N.; Zagorodnikov, V. P.; Stolarov, I. P.; Moiseev, I. I.; Kochubey, D. I.; Likholobov, V. A.; Chuvilin, A. L.; Zamaraev, K. I. *J. Mol. Catal.* **1989**, *53*, 315.

Table VII. Specific Surface Areas ($m^2/g$) of Compounds 4–6

| | 4 | 5 | 6 |
|---|---|---|---|
| a | 0 | 171 | 165 |
| b | 192 | 213 | 224 |
| c | 117 | 315 | |
| d | 0 | 119 | 97 |
| e | 0 | 226 | 229 |
| f | 0 | 222 | 242 |
| f′ | | | 24 |
| g | 0 | 330 | 39 |
| h | 0 | 300 | 35 |
| i | 0 | 657 | 239 |
| j | 86 | 615 | 386 |
| k | 164 | 364 | 181 |
| l | 0 | 373 | 378 |
| m | 0 | 356 | 430 |
| n | 61 | 415 | 504 |
| o | 140 | 606 | 606 |
| p | 229 | 550 | 544 |
| q | 299 | 507 | 484 |
| r | 0 | 450 | 460 |
| s | 82 | 348 | 342 |

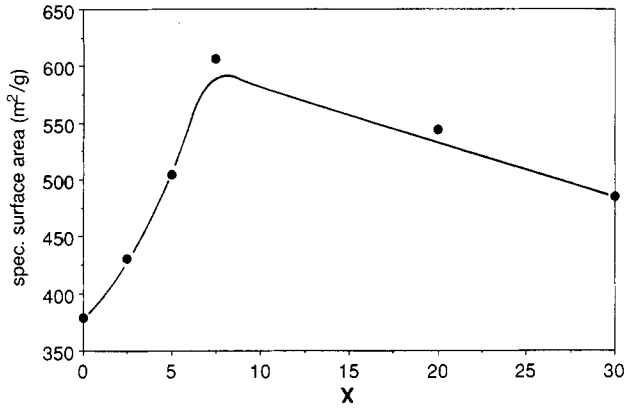


Figure 7. Specific surface area of the PdO composites 5l–q (x are the TEOS equivalents used for preparation of the corresponding polycondensates 4l–q, according to eq 3).

With an increasing portion of 7, the BET surface area of the polycondensates 4 decreases considerably. This effect has already been observed for phosphinoalkylsilyl-containing silica prepared by the sol–gel method and was attributed to an easier network relaxation due to the bulky groups.[14] The polycondensates 4 show porosity only if the TEOS concentration used for their preparation is at least 2–3 times higher than that of 7 (Table VII).

Porosity increases considerably during calcination (Table VII). Burning of the organic moieties obviously increases the surface by generation of pores. However, the surface area of the composites 5 does not linearly depend on the TEOS portion used for preparing the corresponding polycondensates 4, as shown in Figure 7 for 5l–q (a similar dependency is found for 5h–k). We interpret this result as a counteraction of two effects: formation of a stable network from the TEOS portion during polycondensation, and creation of pores by removing of the organic parts. During sol–gel processing (eq 3), the silicate matrix is built around the organic groups provided that sufficient network forming reagent (TEOS) is available. When the organic moieties are burned, the surrounding matrix retains its shape. The surface area increases from 5q to 5o (corresponding to $x = 30$ and $x = 10$) because more pores are formed. With a decreasing amount of TEOS ($x = 5$ to $x = 0$), the polycondensate networks (5o–l) increasingly relax and therefore the surface areas are low or zero. Although the pores are formed upon oxidation, the specific surface area decreases from 5o to 5l due to the increased network relaxation.

Determination of the pore radius distribution by the BET method for the composites 6l, 6n, and 6p supports this interpretation. It shows that in 6l only pores with a radius <1 nm are present. A small percentage of pores with a radius of about 1.8 nm is additionally detected in 6n. Contrary to this, pores of 5–6 nm dominate in 6p, and the number of pores smaller than 1 nm is distinctly lowered.

Surface areas do not change significantly upon reduction of the metal oxide particles, provided that the reduction temperatures are not higher than about 500 °C (Table VII). At 900 °C, the temperature used for the preparation of the Ni-containing composites 6f′ and 6g–k, partial sintering of the $SiO_2$ matrix occurs and results in a decrease of the specific surface area during reduction. This effect is best seen by a comparison of the surface areas of 6f and 6f′.

## Conclusion

Materials containing uniform, nanometer-sized metal particles that are homogeneously dispersed in an electrically isolating $SiO_2$ matrix are prepared by a three-step procedure: In the first step an organically substituted alkoxysilane of the type $X(CH_2)_3Si(OR)_3$ (X = $NH_2$, $NHCH_2CH_2NH_2$, CN) capable of coordinating metal ions, a metal salt with an organic counterion and, optionally, $Si(OR)_4$ are processed by the sol–gel method. In the second step all organic parts are removed by calcination in air, during which very pure and nanometer-sized metal oxide particles develop. Complexation of the metal ions and anchoring the obtained complexes to the silicate matrix in the first step are the keys to obtain a high dispersion of the metal. The small size of the particles is maintained during the final step, in which the metal oxide particles are reduced by hydrogen. Compared with other methods to prepare metal/ceramic nanocomposites, this modification of the sol–gel route provides smaller and more uniform and homogeneously distributed metal particles with a narrower size distribution in an $SiO_2$ matrix. The metal loading can be varied to a high degree, and even with high metal loading, the metal particles are still small, uniform in size, and well separated from each other. The method is applicable to most transition metals, and the present results show that the advantages of this method can be generalized.

**Acknowledgment.** We thank the Bavarian Ministry of Economics, the Deutsche Forschungsgemeinschaft, and the Fonds der Chemischen Industrie for their support of this work, and Mrs. R. Schedl for the DTA measurements and metal analyses.

**Registry No.** $SiO_2$, 7631-86-9; Ag, 7440-22-4; Cd, 7440-43-9; Co, 7440-48-4; Cu, 7440-50-8; Ni, 7440-02-0; Pd, 7440-05-3; Pt, 7440-06-4.

**Supplementary Material Available:** Particle size distribution curves for the composites 6 and pore radii and pore volumes of the compounds 4–6 (Table VIII) (10 pages). Ordering information is given on any current masthead page.

(14) Schubert, U.; Rose, K.; Schmidt, H. *J. Non-Cryst. Solids* **1988**, *105*, 165.